Processes and kinetics of mass gain in archeological brick following drying and reheating

Barrett, G. T. (2017). Processes and kinetics of mass gain in archeological brick following drying and reheating. DOI: 10.1111/jace.14829

Published in:
Journal of the american ceramic society

Document Version:
Peer reviewed version

Title: Processes and Kinetics of Mass Gain in Archaeological Brick following Drying and Reheating

Author Name and Affiliation: Gerard Thomas Barrett, Ph.D.[1]

[14]CHRONO Center for Climate, the Environment, and Chronology, School of Natural Built Environment, Queen's University Belfast, Belfast BT7 1NN, Northern Ireland, UK

Abstract:

The mass gain behavior of archaeological bricks was examined following drying (130°C)/reheating (500°C) and aging at a range of temperatures (25°C, 35°C, 45°C). For drying or reheating, samples exhibit a two-stage mass gain behavior, the second stage, *Stage 2*, continuing indefinitely and better described by a $t^{1/n}$ model ($1/n$ = 1/6-1/2); a correlation between the $1/n$ value and the specific surface area/pore volume demonstrates diffusion mechanisms with some pore geometry/morphology dependence. *Stage 2* is shown to have an Arrhenius temperature dependence with activation energies of similar orders of magnitude following both drying and reheating. Supported by thermogravimetric mass spectrometry (TG-MS), *Stage 2* is demonstrated as likely due to the recombination of chemisorbed water, previously removed, whereas following reheating due to two components, a chemisorbed component associated with drying and a component associated with rehydroxyls removed at higher temperatures during reheating. Differences between activation energies of chemisorption and rehydroxylation components support this. Evidence for a fundamental compositional relationship between these processes is presented by a strong linear relationship between the drying and reheating mass gain rates. *Stage 1*, following drying or reheating, is shown to be likely associated with physisorption processes alone.

I. Introduction

Understanding the mass gain behavior of fired clay ceramics is crucial to the future of rehydroxylation (RHX) dating, an archaeological approach that exploits the mass gained (due to uptake of environmental moisture) since original firing to provide an estimate of a ceramic's age (e.g. Wilson et al.[1,2]). Following original firing or reheating (500°C), mass gain in the fired clay proceeds by two consecutive stages, *Stage 1* and *Stage 2*.[1-4] The first of these, *Stage 1*, is a

[1] Email: g.barrett@qub.ac.uk

more rapid initial mass gain that commences following exposure of the fired/reheated ceramic to environmental moisture and is completed on the order of hours, typically.[1-4] *Stage 2* is a long term (minimum of months) mass gain that was originally argued to be suitably described by a $t^{1/4}$ model.[1-4] The underlying $t^{1/4}$ process also commences with exposure to environmental moisture and, therefore, is underway during *Stage 1* but continuing in *Stage 2*.[1-4]

For archaeological dating the following properties are central: (1) the *Stage 2* mass gain is adequately described by a $t^{1/4}$ model[1-4], and (2) the mass gain equilibrates to a constant value (used in age estimation calculations) within a short period (days), following drying at 105-110°C.[1,2] However, there is growing evidence against the suitability of a $t^{1/4}$ model, with instead a more flexible $t^{1/n}$ model argued to provide a better description.[5-9] There have also been issues encountered with equilibration following drying (drying herein generally refers to the process of oven heating of a previously fired ceramic at 105-130°C to remove loosely bound or physisorbed water); the mass gain has been observed to have a two stage behavior, similar to that following reheating at 500°C (reheating herein refers to heating of a previously fired ceramic at 500°C), with the second of these, *Stage 2*, again more adequately modelled by a $t^{1/n}$ based approach.[7-10] A review of RHX work has further found that these properties, (1) and (2), are not adequately supported by experimental evidence and are questionable in their suitability (see *Section 2.5* of Barrett[11]). For continued development of RHX dating, these properties need further clarification.

An improved understanding of the processes contributing to *Stage 1* and *Stage 2* following both drying and reheating would be beneficial in this regard. While there has been detailed work on understanding the nature of chemically bound water in clays and the effect of heat on the clay mineralogy and microstructure, reviewed elsewhere[11,12,13], the mechanism and kinetics of mass gain following reheating that lead to this *Stage 1* and *Stage 2* behavior are still not well understood (see review of Hamilton and Hall[13] as well as the discussion of Gallet and Le Goff[10]); in terms of physisorption on fired clays (specifically aluminosilicate rich and compositionally complex archaeological ceramics[14-16]), with the exception of studies on related, but more homogeneous, materials[14] and more recent RHX related studies[17,18], there appears to be a a dearth of focused work.

The present work defines *Stage 1* as the non-linear (as a function of $t^{1/4}$ or $t^{1/n}$) initial period of rapid mass gain following firing or reheating. The *Stage 1* mass gain, m_{S1}, is defined as the mass gain which occurs during *Stage 1* that is not attributable to the $t^{1/4}$ or $t^{1/n}$ process that is continuing in *Stage 2*. *Stage 2* is defined as the subsequent period over which mass gain is linear as a function of $t^{1/4}$ or $t^{1/n}$.

Wilson et al.[2,17] define three types of water associated with mass loss during reheating that lead to the subsequent *Stage 1* and *Stage 2* mass gain: *T0* being physisorbed water removed at 105°C; *T1* being chemisorbed[2] or physicochemically (weak chemical) bonded[17] water removed between 105°C-500°C; and *T2*, the (re)hydroxyls, removed at 500°C. It is argued by Wilson et al.[2,17] that, following reheating, *Stage 1* mass gain is due to a combination of both *T0 + T1* water, termed *T01* water, as well as simultaneous *T2* (rehydroxylation mass gain); *Stage 1* ends with equilibration of *T01* water with *Stage 2* then commencing with continued uptake of *T2* water alone (following drying at 105°C, equilibration of *T01* physisorbed water is the only mass gain process taking place[2]). Yet the arguments for associating a distinct chemisorbed or weakly chemically bonded water, *T1*, with *Stage 1* do not appear well justified[11] with Gallet and Le Goff [10] instead arguing for associating *T1* with a chemisorption process taking place in *Stage 2* following both drying and reheating (for the latter they argue that chemisorption and rehydroxylation processes may be taking place).

The present work, part of a larger study assessing the archaeological application of rehydroxylation dating,[11] attempts to clarify (a) the nature of the processes in both stages, (b) the suitability of the aforementioned mass gain models, and (c) the manner of mass gain following drying. For a diverse collection of well-fired pre-dominantly post-medieval brick samples, the mass gain curves obtained following both drying and reheating and also for a range of aging temperatures are recorded and analyzed with both mass gain models tested (*aging* refers to the sample gaining mass, following drying/reheating, under constant environmental conditions, i.e. temperature and humidity). As well as this, surface area analysis (BET) and thermogravimetric mass spectrometry (TG-MS), are conducted.

II. Experimental Procedure

Samples and Preparation

The sample set consisted of 18 samples of brick and pottery. These were pre-dominantly post-medieval structural bricks from Ireland (14), but also include post-medieval Irish pottery and a piece of Etruscan and Roman pottery (see details in supplementary materials, *Table S1* with further information in Barrett[11]). The samples were characterized using XRD, FTIR, XRF, p-XRF, and petrographic analysis[11]; identification of minerals associated with high temperature firing (see *Table S2*), e.g. cristobalite, spinel, mullite (see Dunham[19]) suggest that, with the clear exception

of the Etruscan (*Etr*) and Roman *(Rom*), samples were likely to have been well-fired above 850°C, certainly above temperatures, 400-800°C, required for dehydroxylation of most clay minerals[19,20] (see also review of dehydroxylation temperatures provided in Table 2.3 of Barrett[11]). Additionally, from petrographic analysis (*Table S3*), evidence for partial vitrification (bloating/melting) was common in brick samples.

Samples were (wet-)cut into sets of cubes (20-40g, or subsherds) with outer layers removed (2-4mm), cleaned (rinsed with de-ionized water), granulated (chiseled by hand and sieved to extract granules of size 2-5.6mm, 0.05-0.15g), and given a final cleaning; pre-drying at 60°C was carried out at various stages during this process to remove both loose water introduced during preparation and bulk water already in the sample before proper drying was conducted. Granulation was carried out in order to allow mixing and homogenizing of sample material that often has a very heterogeneous composition in its original form. These granules were thoroughly mixed and would eventually be split into three subsamples (15-25g) per sample after drying. These three subsamples would then be aged at 25°C, 35°C or 45°C after both drying and reheating.

Drying, Heating and Mass Gain

Granulated samples were dried at 130°C in an oven over a period of 2 months (full method and issues of incomplete drying are discussed elsewhere[11]). On the penultimate day of drying, splitting into subsamples was conducted; subsamples were placed into Pyrex beakers before a final day of drying.

Following drying, the 130°C stage of mass gain measurements were performed. Subsamples to be aged at 25°C were cooled in desiccated container (pre-conditioned to < 3%RH, silica gel) before transfer to a glove box arrangement (see Barrett[12]), GBA, which features a top-loading balance (*Sartorius CPA225D*, 100g capacity, ±0.02mg repeatability) under controlled temperature (25 ± 0.5°C) and humidity conditions (75 ± 1%RH). The *Stage 1* mass gain was recorded over a period of 6-7 hours before the subsamples were moved to an environmentally (temperature) controlled chamber (25°C), ECC, with humidity controlled by saturated salt solution of NaCl (75 ± 1%RH experimentally determined, see Greenspan[21]) in a sample box holder used for storage and transfer to/from the glove box arrangement. The samples were then transferred for periodic weighing to the GBA over a minimum period of two months (initially daily but with growing intervals as the quantities of mass gain diminished). The procedure for

the samples aged at 35°C and 45°C is identical except *Stage 1* monitoring was not carried out and the environmental chambers were at the respective aging temperatures.

After the 130°C stage mass gain monitoring was completed, the subsamples were heated in a furnace at 500°C for a period of approx. 72 hours. Then the same procedure as for the 130°C stage was repeated (after reheating samples were let cool to 200°C in the furnace before removal to desiccated conditions) with weighing conducted over the same duration.

Mass Gain Curve Analysis (*Stage 1*)

The main characteristics of interest in *Stage 1* are the mass gain, m_{S1}, across the duration, t_{S1}, of *S1* and the differences between the dried (130°C) and reheated (500°C) components of this property, see *Figure 1 (a)*. The mass gain during *S1*, m_{S1} is calculated from the difference in the intercept mass, m_0, acquired through modelling of the *S2* mass gain with the $t^{1/4}$ model (see below), and the initial (dry) mass gain measurement recorded for *S1*, m_d. This value was then normalized with respect to m_d to provide a fractional value for comparison between samples. Estimation of the *S1* mass gain is not precise and can only be taken as an approximation; the first measurement during mass gain measurements will not correspond to the initial 'dry' mass, m_d, as a significant level of moisture uptake (physisorption/chemisorption) will have taken place already (dependent on timing delays, variations in %RH control/temperature, type of sample, i.e. surface area). Also, because the completed *S1* mass estimates, m_0, are based on the $t^{1/4}$ modelled results, the results are taken only as an approximation and proxy for the true *S1* mass gain.

Mass Gain Curve Analysis (*Stage 2*)

The *Stage 2* mass gain was modelled using the following generalized expression:

$$m(t) = \propto_m (T) t^{\frac{1}{n}} + m_0 \qquad (1)$$

with $m(t)$ the sample mass, t the time since exposure to moisture following drying/reheating, m_0 the intercept mass of the *S2* mass gain, α_m the mass gain rate (elsewhere referred to as the rate constant[1,2]), T is the absolute temperature, with $n = 4$ or $n = r$, with r sample dependent.[1,2,5,7] Where $n > 4$ or $n < 4$, the *Stage 2* mass gain is referred to as having a *positive* or *negative* curvature, respectively, *Figure 1 (a)*.

The mass gain rate (rate constant) has an Arrhenius temperature dependence[1] and can be described by the following equation (generalized from Hall and Hoff[22]; Hall et al.[23]):

$$\alpha(T) = Ae^{-\frac{E_a}{nRT}} \quad (2)$$

with A the pre-exponential factor, E_a the activation energy, R the gas constant, T the absolute temperature, and $n = 4$ for $t^{1/4}$ model.

Where the rate constant is estimated for a range of temperatures, the activation energy can be calculated from:

$$\ln\left(\frac{\alpha}{\alpha_0}\right) = -\frac{E_a}{nRT} + \frac{E_a}{nRT_0} \quad (3)$$

with α_0 the rate constant at some reference temperature T_0. Plotting the natural log of the normalized rate constant (normalised relative to the reference rate) as a function of the inverse temperature and then carrying out a linear regression, permits the activation energy to be calculated from the slope.

Modelling

The mass gain curves were modelled using custom code featuring the *MATLAB R2012a* function *fit* at its core (linear and non-linear least square regressions using a Trust Region algorithm). A timespan analysis (an approach previously used by Le Goff and Gallet[8]) was carried out that involved modelling all data points initially and then consecutively subtracting a data point from the start of the previous series for each subsequent regression; best-fit R^2 and *RMSE* values were recorded as a function of this process. However, because of issues with curvature in the data for the $t^{1/4}$ approach, and in order to provide a standard period of comparison, modelling was generally carried out over the entire ECC-GBA measurement period. For $t^{1/n}$ modelling, this timespan analysis was used for each of the six data series associated with each sample (130°C/500°C, three temperatures). Each best fit provided a value for 1/*n*. The average of these was taken to provide a constant 1/*n* value, 1/*r*, say with a $t^{1/r}$ model then re-applied to all six data series. Fixing 1/*r* assumes conformity to a fixed 1/*n* behavior for all drying/reheating and aging temperature curves; however for *abnormal* samples that suffered from high surface area capillary condensation issues (*Etr*, *Por*, *Lan*, *Dow1*, *Dow2*, and *Rom* to some extent), discussed in Barrett,[11] modelling with a $t^{1/n}$ approach was unsuccessful. Mass gain rates were normalized relative to the intercept mass of the 500°C *Stage 2* curve, m_{500}. The RHX rate, α_{RHX}, was calculated for each aging temperature by subtracting the 130°C curve rate, α_{130}, from the 500°C curve rate, α_{500}, *Figure 1 (b)*;

this component based approach is dealt with elsewhere. This was carried out for both the $t^{1/4}$ and $t^{1/n}$ models (see Barrett[11], Section 7.2 for worked examples and for more detail on modelling method, results and the component based approach).

Activation energies were calculated (*Equation 3*), for both the 130C (E_{a130}) and 500C (E_{a500}) components separately, and also for the RHX component, E_{aRHX}, using the RHX rate constant estimates. Again this was carried out for both the $t^{1/4}$ and $t^{1/n}$ approaches, where possible.

TG-MS and Sorption (BET) Analysis

Thermogravimetric-mass spectrometry was carried out using a *Netzsch TG 209 F1 Libra* thermo-microbalance in series with a *Pfeiffer Thermostar* mass spectrometer. Approximately 30-40mg of powdered dating sample (<63μ) was placed in an Al_2O_3 crucible within the *TG 209* and heated from 25°C to 1000°C at a rate of 20°C/min under a constant flow of nitrogen at 50mL/min. Mass spectrometry was carried out for ions of mass number 18 (H_2O), 44 (CO_2) and 64 (SO_2) with only the results for mass 18 dealt with in the present work. Sampling of the mass and ion current (mass spectrometry) was carried out for each °C increment in temperature. Analysis of the mass loss curve, its first derivative, and ion fragment curves was undertaken after smoothing (moving average with n = 11). For comparison, the mass loss (%wt. loss) and mass spectrometer (mass18, H_2O) ion current (A) curves were scaled to match the total mass loss and ion current of the sample *Ann* over the region 50-600°C. An average H_2O loss curve for well-behaved (see *Discussion*) samples was prepared.

Adsorption tests were carried out to examine the specific surface area (S.S.A., Brunauer-Emmett-Teller (BET) theory) and pore size/volume (Barrett-Joyner-Halenda, BJH theory) of samples.[24] This was carried out by the facility *Analytical Services and Environmental Projects (ASEP)* at Queen's University Belfast using a *Micromeritics Tristar II 3020* automated gas (nitrogen) adsorption analyser. Approximately 0.5-0.8g of granulated sample (3.35-2mm sieved fraction) was submitted for analysis for each sample. This followed heating of the sample at 500°C for 24 hours to remove most bulk moisture and combustibles from the sample that might interfere with the adsorption/desorption processes. Issues were encountered with samples *Rat* and *Tur* where sorption was particularly low and complete sorption curves could not be recorded for estimation of all surface area related characteristics (*Cal* also presented poor sorption curves due to low surface area). Note that BET was carried out on a couple of granules

and will not have the level of homogeneity of the samples used in mass gain experiments i.e. the results reflect more localized characteristics in the original material.

III. Results

Curves

The complete set of *S1* and *S2* mass gain curves and modelling results is available in Barrett.[11] Several examples of the different types of behavior encountered are presented below in *Figure 2* (normalized with respect to m_0 of the respective *Stage 2* modelled fit). The first two plots, *top left* and *top right*, present the curves for *Ann* and *Esp* and are typical of *well-behaved* (see *Discussion*) samples (12/18 samples) that exhibit an *approximate* $t^{1/4}$ behavior and an Arrhenius temperature dependence in *Stage 2*, see *Figure 3* (*a*,*b*,*c*). A feature of well-behaved samples, the *S1* mass gain, m_{S1}, is of a very similar magnitude for both the 130°C and 500°C components and the duration, approx. 1.5 hours, has normally completed within 24 hours. The examples, *Figure 2 (middle left* and *right), Lan* and *Rom* are *abnormal* samples (6/18 samples) that display very long *S1* duration, 165-195 hours, typical of samples with poor *Stage 2* linearity and poor Arrhenius temperature dependence, *Figure 3* (*d*). The magnitude of *S1* is large, approx. 1% of ceramic mass, characteristic of abnormal samples, whereas well-behaved samples are normally less than 0.1% (see Barrett,[11] *Section 7.6.2*).

The example *Rat, Figure 2* (*bottom left*) is unusual because it exhibits no *S1* behavior and a strong *positive* curvature. *Mac*, (*bottom right*), like *Bel*, shows *S1* behavior that is significantly greater in magnitude (approximately x4 times) for the 130°C component than for the 500°C component. This is related to the presence of gypsum, dealt with elsewhere.[11]

Examples of typical sets of curves for all aging temperatures are provided in *Figure 3*. The first three examples (*a*-*c*) correspond to well-behaved samples with (*d)* corresponding to an abnormal sample. For well-behaved samples, it can be observed that there is an approximate $t^{1/4}$ linearity to *Stage 2* and a clear temperature dependence as a function of the aging temperature. Also this behavior can be observed following both drying (blue) and reheating (red). For abnormal samples, the prolonged *Stage 1* is still taking place, distinguishing a temperature dependence is difficult, the *Stage 2* linearity is not as sharply defined (on-going curvature) and there is large scatter in the data which made

modelling difficult, if not impossible. For well-behaved samples, the *Stage 2* mass gain as a function of $t^{1/4}$ shows a clear curvature for all aging temperatures, and following both drying and reheating.

Stage 1

The relationship between the 130°C and 500°C *S1* mass gains (at 25°C aging temperature) are presented in *Figure 4 (a);* abnormal samples plus *Cau* are removed because of modelling issues, and *Mac* and *Bel* because of gypsum related physisorption issues.[11] Negative mass values result from the m_0 modelled values of samples with positively curved (upward concave) *S2* and very small m_{S1} being less than m_a. As this issue affects the estimates from both the drying and reheating curves to a very similar degree (because the magnitude of curvature is the same for both, shown later), comparing the 'proxy' *S1* fractional masses of both is considered acceptable. Observation of the mass gain curves alone, see examples in *Figure 2* and the complete set in Barrett (*Appendix E*),[11] reveals little difference between the *S1* magnitudes following drying and reheating.

Rates, Activation Energies and 1/n Values

The relationships between the fractional mass gain rates following drying and reheating (i.e. the 130°C and 500°C components) at each aging temperature, are shown in *Figure 4 (b),* for the $t^{1/4}$ model (the $t^{1/n}$ model produced similar results, *Figure S5*). For the $t^{1/4}$ plots, the six abnormal samples have been removed. Strong linear relationships with slopes of similar magnitude are apparent for all aging temperatures (mass gain rate and intercept data is included in *S11-S14*).

An example of the Arrhenius plot used in activation energy estimation is presented in *Figure 4 (c)* for *Ann* using the $t^{1/4}$ model. Linearity is present for all components (130°C, 500°C and RHX); this is typical of normal samples and the same for use of a $t^{1/n}$ model (*Figure S6*). Bar charts of the samples' activation energies for drying and reheating are displayed in *Figure 5 (a),* using the $t^{1/4}$ model. Activation energies are very similar for both components, 130°C and 500°C, using the $t^{1/4}$ model, with the exception of *Nic* and *Mac* where differences of > 40kJ/mol are observed. Similar behavior was observed for the $t^{1/n}$ model results (see *Figures S7-8*). Any differences between the 130°C and 500°C activation energies are statistically insignificant, with the exception of *Nic* and *Mac*. RHX activation energies are presented in *Figure 5 (b)* (tabulated data is included in *S15-S16*).

In terms of typical behaviour, the average activation energies (and standard deviation) are as follows for $t^{1/4}$ model: $E_{a130}(avg) = 70 \pm 35$ *kJ/mol*; $E_{a500}(avg) = 77 \pm 40$ *kJ/mol*; $E_{aRHX}(avg) = 109 \pm 74$ *kJ/mol*. The large spread in values accounts for the large standard deviation. If abnormal samples are excluded, the values are: $E_{a130}(avg) = 78 \pm 31$ *kJ/mol*; $E_{a500}(avg) = 86 \pm 35$ *kJ/mol*; $E_{aRHX}(avg) = 137 \pm 70$ *kJ/mol*. For $t^{1/n}$ the values are as follows: $E_{a130}(avg) = 58 \pm 14$ *kJ/mol*; $E_{a500}(avg) = 67 \pm 26$ *kJ/mol*; $E_{aRHX}(avg) = 101 \pm 78$ *kJ/mol*. With abnormal samples removed, this becomes: $E_{a130}(avg) = 58 \pm 14$ *kJ/mol*; $E_{a500}(avg) = 72 \pm 19$ *kJ/mol*; $E_{aRHX}(avg) = 109 \pm 75$ *kJ/mol*.

In *Figure 6 (a)*, a chart compares the average 1/*n* values (separate averages of the three modelled aging temperature curve 1/*n* values for both drying and reheating) of the samples together with the uncertainties (tabulated data *S17*). The curvature is predominantly positive ($n < 4$) and there is a good agreement between the behaviour of the 130°C and 500°C groupings for each sample (*t*-test of paired samples, $p = 0.20$, the null hypothesis of no difference between pairs cannot be rejected).

Surface Area

The results of BET surface area analysis are presented in *Figure 6 (b)* with tables of surface area and pore size/volume measurements provided in the supplementary data, *Table S10*. For *Rat*, the specific surface area was negligible. A strong correlation, $R^2 = 0.91$, between BET surface area and the fractional *Stage 1* mass gain (using the average of the 130°C and 500°C components, $m_{S1\text{-}avg}$ (fract.)) is presented in *Figure 6 (c)* for all samples and using the $t^{1/4}$ model (similar results, *Figure S9*, for the $t^{1/n}$ model). An association between BET surface area and the 1/*n* value of well-behaved samples is explored in *Figure 6 (d)*. Some relationship between the two is probable, $R^2 = 0.76$ and with a *p-value* = 0.0002 (*t*-test of the null hypothesis of the slope equating to zero).

In relation to the magnitude of the surface area and its relationship to well-behaved or abnormal samples, a brief note can be made. Well-behaved samples that produced strongest evidence of having been originally fired at higher temperatures (*Table S2-3*) tend to have low surface area values, likely due to a reduction or closing of pores with vitrification/melting.[25] The high surface area of *abnormal* samples (*Lan, Etr, Rom, Dow1, Dow2, Por* and *Cau* to a lesser extent, often in excess of 14m^2/g, see *Figure 6 (b)*) can be associated with low temperature firing for some samples (e.g. *Etr, Rom*) but for others (*e.g. Dow1, Dow2*) the formation of, for example, wollastonite and anorthite (*S2*, 800-1050°C firing temperature, see Dunham[19]) suggests they were well-fired. For these *abnormal* samples, the role of calcite and its thermal products (particularly poorly decomposed primary calcite, recrystallized calcite or

secondary calcite) are suspected to be involved in the high surface area values but more work on this topic is required (a detailed discussion is provided in Barrett[11]; note however the strong presence of calcium rich minerals in these samples, *S2-3*, as well as the high calcium levels (CaO) in abnormal samples, included in table *Table S4*, using p-XRF analysis).

TG-MS and Water Loss

The complete set of TG-MS curves are provided in Barrett (*Appendix C*),[11] with mass spectrometry examples provided in *Figure 7*. A summary of the major features identified and related to moisture loss for all samples are shown in *Table 1*. This table is divided into *Events A-D*, which correspond to removal of mass 18 ions (H_2O) within the following temperature ranges: *A =50-100°C; B=100-180°C; C=210-280°C; D=300-380°C.* Events *B, C, D* are often identified in pairs (*B* & *C* or *B* & *D*) with *B* and *D* most common; these events are generally very broad features, lacking clear or well defined boundaries, as observable in *Figure 7*. For abnormal samples (associated with high surface area) a strong peak was present at temperatures just below 100°C and this made the presence/absence of *Event B* difficult to confirm; its absence in *Table 1* may reflect this.

The average water loss (MS H_2O ion current) for 10 well-behaved samples (black line, *Mac* and *Bel* excluded) is presented in *Figure 7*, together with examples of the individual curves for *Rat* (red dotted) and *Ann* (green dashed). Three main features are strongly represented in the average behaviour curve, a peak at approximately 65-70°C (removal of physisorbed water), and two broad structures at higher temperatures with peaks at approximately 150-160°C (*Event B*) and 300-310°C (*Event C/D*). As is made clear in *Table 1* and the examples *Rat* and *Ann*, included in *Figure 7*, the location of these structures varies to a moderate extent dependent on the sample, with the averaged curve interpreted as representative of the more typical behaviour. Note the low levels of moisture removal below 100°C relative to that above for the sample *Rat*; this was typical of well-behaved samples (e.g. *Tur*) which exhibited low BET surface area. The exclusion of *Mac* and *Bel* from the average behavior curve was due to the presence of a very strong and narrow peak at approximately 90°C which when included in the averaged curve obscured other structures nearby; this behavior for *Mac* and *Bel* is associated with gypsum related issues, mentioned previously.

IV. Discussion

***Stage 1* and Physisorption**

Despite the need for a more accurate means of estimating the *Stage 1* mass gain, a strong argument for an interpretation of the *Stage 1* mass gain (excluding an on-going $t^{1/n}$ or $t^{1/4}$ process) resulting solely from physisorption of water on the surface/pores of the ceramics can be made:

1. The magnitude of the *Stage 1* mass gain, m_{S1}, following both drying and reheating are very similar if not identical (exceptions being *Mac* and *Bel* where gypsum effects are involved[11]), see for example *Figure 2* and *Figure 4 (a)*. Also, the increase in the *Stage 2* mass gain rate, *Figure 4 (b)*, following reheating (of the order of 25-30%) is not accompanied by any definitive change in the *Stage 1* behavior.
2. There is a very strong correlation, $R^2 = 0.91$, between the BET surface area and the quantity of *Stage 1* mass gain, *Figure 6 (c)*. This is demonstrated most definitively for the sample *Rat* for which both the BET surface area, *Figure 6 (b)*, and *Stage 1* mass gain, *Figure 2*, were negligible. Note also that this absence of observable *S1* mass gain is independent of the significant chemisorption and rehydroxylation processes taking place in *S2*, *Figure 2*.
3. The *Stage 1* mass gain is associated with the removal of *Event A* (removal of mass 18 ions, i.e. water) in the TG-MS data in the temperature regimes 50-100°C. This is supported by the very low levels of this event for samples that displayed both low BET surface area and *Stage 1* mass gain, i.e. *Rat* in *Figure 7*, and high levels for samples with high surface area and *Stage 1* mass gain, i.e. *Etr*.

The argument by Wilson et al.[2,17] that *Stage 1* is associated with both physisorbed (*T0*) and weakly chemisorbed or physicochemically bonded (*T1*) water, the latter removed during heating at 200-300°C, does not appear justified in the present work. While the process(es) responsible for *Stage 2* $t^{1/n}$ mass gain (chemisorption/rehydroxylation) is (are) on-going over the duration of *Stage 1*, the present work supports an interpretation of the defined *S1* mass gain, m_{S1}, being solely attributable to physisorption. The strong relationship between *Stage 1* mass gain and specific surface area does provide the first convincing evidence that there is a correlation between the specific surface area and duration of *S1*.[17] Particularly, it can be observed in the prolonged *Stage 1* duration of high surface area samples, for example *Lan* and *Rom* in *Figure 2* and *Figure 3* (This is examined more in Barrett[11] where a correlation of $R^2 = 0.89$ is found between the magnitude and duration of *S1*). The previous argument for the correlation between specific surface area and duration (Wilson et al.[17]) suffers from several issues (critiqued previously[8,11]): there is disagreement between their plot (Figure 7) and the table of data used (Table 2), with a data point omitted without explanation and another

appearing to be assigned an incorrect value; the plot is also biased positively by a single sample with a large specific surface area.

Drying (130°C) and chemisorption

An on-going mass gain, *approximately* linear as a function of $t^{1/4}$, following drying has only recently been reported by Le Goff and Gallet,[7,8] Gallet and Le Goff,[10] and Zhao et al..[26] Previously, Wilson et al.[1,2] reported equilibration following drying at 105°C, requisite to the original RHX dating methodology. Le Goff and Gallet,[8] in a re-examination of Wilson et al.,[2] found that equilibration questionable. The present work provides independent evidence in support of both Le Goff and Gallet and Zhao, finding this on-going *Stage 2* $t^{1/n}/t^{1/4}$ behaviour for a large set of samples (54) and for aging at three different temperatures, e.g. *Figure 2* and *Figure 2*. Additionally, this work provides more direct evidence that the behaviour is chemically driven (agreeing with the conclusions of Gallet and Le Goff[10]), with a clear Arrhenius temperature dependence for the 130°C component, e.g. *Figure 4 (c),* and activation energies of an order similar to those obtained for the 500°C component (average for well-behaved samples 78 ± 31 kJ/mol (130C) and 86 ± 35 kJ/mol (500C), respectively), *Figure 5 (a),* but seemingly lower than those associated with rehydroxylation, 137 ± 70 kJ/mol, *Figure 5 (b)* (accepting that the latter suffer from large uncertainties). These values agree with activation energies in the range 40-182kJ/mol that have previously been reported and associated with rehydroxylation.[1,12,20,27,]

Well-behaved samples generally displayed clear evidence of *Event B* in the TG-MS data, *Table 1* and *Figure 7*. This event (peaking in the range 150-160°C) is not due to removal of physisorbed water, for which an independent lower temperature peak, *Figure 7*, is present. It is now suggested that *Event B* might be a low-temperature chemisorption event which results in the removal of chemisorbed water during drying and is reversible to some extent during post-drying mass gain; this results in a 130°C *Stage 2* mass gain component with a corresponding activation energy of average value 78kJ/mol for the present set of samples. This *Event B* finds support elsewhere in the 'bump' below 300°C in the dilatometry results of Gallet and Le Goff[10] (Figure 6), which they also associate with the removal of chemisorbed water. This peak may correspond to chemisorbed water removed between 105-300°C that is described by Drits and McCarty[28] (see also Clegg et al.[18]). This chemisorption process may explain an issue of prolonged drying of samples with low surface area, even after two months of heating at 130°C, mass loss was on-going (Barrett[11]); this drying temperature sits below the peak removal temperatures recorded in the TG-MS (typically 150-160°C) and may thus only permit removal of chemisorbed molecules at a less than optimal rate. In Barrett, the only well-behaved

sample to fully dry was *Esp* for which *Event B* was very low in magnitude and with a peak water removal temperature of 110°C, well below the drying temperature of 130°C (prolonged drying of abnormal samples, for which *Event B* is hard to identify in the TG-MS data, possibly masked by the large peak associated with removal of physisorbed water, was also an issue; however, these samples have a considerably greater capacity for water (high surface area and pore volume) and drying may be prolonged for this reason also). The above evidence for the existence of a chemisorption event, distinct from a higher temperature rehydroxylation event, agrees with Gallet and Le Goff [10] who come to a similar conclusion based on the variation of 1/*n* with the drying/reheating temperature.

Examination of the 130°C mass gain rates, $\alpha_{130\text{-}25/35/45}$, and the 500°C mass gain rates, $\alpha_{500\text{-}25/35/45,}$ at each aging temperature could be significant in suggesting a strong relationship between the low temperature chemisorption event and higher temperature rehydroxylation event. With the abnormal samples removed (and additionally *Cau* for $t^{1/n}$ because of modelling issues discussed earlier), the correlations between both components mass gain were extremely strong (ranging from R^2 = 0.94-1.00) at all aging temperatures, *Figure 4 (b)*. As well as this, the ratios (slope of the linear fits) between $\alpha_{500\text{-}25/35/45}$ and $\alpha_{130\text{-}25/35/45}$ rates were very similar for each of the three aging temperatures, (ratios of 1.26, 1.29, 1.25, for $t^{1/4}$ model, and 1.31, 1.25, 1.27, for $t^{1/n}$). This relationship appears to be independent of the sample. Based on this the following interpretation is proposed for discussion/examination:

Mass gain (*S2*) following heating at 130°C is due to recombination of water associated with a low temperature chemisorption event, *Event B*, and mass gain following heating at 500°C is due to recombination of water associated with this event plus recombination due to a high temperature chemisorption event, *Event C/D* (rehydroxylation). The rates of mass gain are proportional to the number of low/high temperature chemisorption sites available for recombination, with *Event C/D* having approximately 25-31% (from ratios above) of the number of sites that are available for *Event B*. This relationship holds across 12 samples, suggesting both chemisorption events are associated with a shared compositional feature (speculatively a fully/partially dehydroxylated clay mineral), present in all samples, in which the ratio of high and low temperature chemisorption sites is structurally determined and approximately constant. A more thorough discussion of this can be found in Barrett.[11]

Stage 2 and a $t^{1/n}$ Model

From examination of the mass gain curve examples in *Figure 2* and the combined modelled 1/*n* results in *Figure 6 (a)*, it is clear that the curvature in *Stage 2* is both present and a property of the sample, varying from approx. 1/6 -1/2

(0.16-0.45) for the average 1/*n* value of a sample. The 1/*n* value is generally >1/4 for well-behaved samples. Only samples *Rom*, *Bel*, *Nic*, *Cau*, and *Esp* are <1/4 (excluding *Esp*, various issues with these samples, particularly with regard to curve modelling, arose and are discussed elsewhere in greater detail (Barrett[11]); in brief, they tend to suffer from a prolonged *Stage 1* which in turn made *Stage 2* modelling more problematic due to fewer data points and the discrimination of the commencement of *Stage 2*).

Perhaps the strongest support for the curvature being real (i.e. not an experimental artefact[17], a point dismissed elsewhere on account of suitable experimental design[10,11]) is that, with the exception of *Mac* and *Cau*, the 1/*n* values for the different heating temperatures (130°C and 500°C components) and aging temperatures of the subsamples agree well with one another, while at the same time differing from other samples that experienced identical treatment and aging conditions. The range of 1/*n* values, from approx. 1/6-1/2 for all samples, and from approx. 1/5-1/2 with problematic samples (Rom, Bel, Nic, Cau) excluded, agrees well also with those observed in previous work: Le Goff and Gallet[7,9] provide convincing evidence that the mass gain behavior may be better described by a $t^{/n}$ model with 1/n varying from 1/6-1/3 or 1/4-1/2, respectively; Gallet and Le Goff found that the 1/*n* value varied dependent on the drying/reheating temperature and they suggest theoretically defined limits of 1/2 – 1/4 that are governed by the diffusion mechanisms present.[10] A *t-test* of the null hypothesis that the 130°C and 500°C 1/*n* values (average of 25°C,35°C,45°C aging temperatures) are the same produced a *p-value* of 0.20. Therefore the null hypothesis cannot be rejected and within the uncertainty limitations of the present work no difference associated with drying/reheating temperature can be distinguished. The author accepts that difference may exist and might be masked by the magnitude of uncertainties or that the two heating temperatures chosen (130°C and 500°C) lead to *Stage 2* mass gain behaviors with similar 1/*n* values (a possibility given the nature of the curve in Figure 5 of Gallet and Le Goff). Similarly, there is no evident aging temperature dependence to the magnitude of 1/*n*.

The relationship of the level of 1/*n* with the BET surface area was briefly examined, *Figure 6 (d)*. There is a strong correlation, $R^2 = 0.76$ ($p = 0.0002$). Note that this was found to increase to $R^2 = 0.89$ when only positive curvature samples were used. This relationship between curvature and surface area has previously been highlighted and discussed by Wilson et al.,[17] however they explained the deviation from a $t^{1/4}$ model as due to both experimental effects and prolonged *Stage 1*; this explanation has already been dismissed for the present work with a more thorough discussion of why it is not valid found in Barrett.[11] The relationship might instead suggest a connection, via the

specific surface area and pore volume, between the $t^{1/n}$ diffusion mechanism associated with mass gain and the pore structure of the ceramic. More work is needed to support and elucidate why samples with lower surface area and lower pore volume, might have higher $1/n$ values that can be associated with freer diffusion within the available pore structure of the ceramic body, i.e. a more Brownian-type $t^{1/2}$ diffusion; perhaps high levels of physisorbed water associated with high surface area samples are inhibitive in some sense, resulting in more one-dimensional $t^{1/4}$ type diffusion.

In any case, the mass gain in fired clay ceramics obeys, or is more adequately described, by a $t^{1/n}$ model with $1/n$ variation dependent on the diffusion pathways, more specifically the micropore structure, of the sample. Certainly, it no longer seems tenable to constrain the behavior to a $t^{1/4}$ model.

V. Conclusion

Data from a large set of mass gain curves (54), obtained following drying (130°C) and reheating (500°C) with subsequent aging at three different temperature (25,35,45°C), was examined together with BET surface area and TG-MS data. For the diverse collection of samples used (archaeological material, mostly post-medieval brick), a better understanding of the mass gain behavior and associated physisorption/chemisorption processes, with particular relevance to RHX dating, has been gained in the form of the following findings:

- *A two-stage mass gain follows drying, with similar behaviour to that following reheating at 500°C:*

  Following drying (130°C), well-behaved samples exhibited a two-stage mass gain behavior: a *Stage 1* mass gain profile almost identical to that following reheating at 500°C; and a *Stage 2* behavior similar to that following reheating at 500°C also, i.e. having the same $t^{1/n}$ behavior but with lower rate mass gain rates.
- *The Stage 1 mass gain is due to physisorbed water:*

  The *Stage 1* mass gain (not associated with $t^{1/n}$ behaviour) for both the 130°C and 500°C mass gain curves is due exclusively to physisorbed water, evident in its correlation with surface area/pore volume, its similar magnitude following 130°C and 500°C heating, and its strong association with the removal of physisorbed water in TG-MS data.
- *The Stage 2 mass gain of the 130°C component has an Arrhenius temperature dependence, and is associated with a (low temperature) chemisorption event*:

The *Stage 2* mass gain behavior was found to have an Arrhenius temperature dependence for both the 130°C and 500°C mass gain curves. The average activation energy of the 130°C (78kJ/mol or 58kJ/mol, model dependent) process was slightly lower than that following heating at 500°C (86kJ/mol or 67kJ/mol), but significantly lower than the estimated RHX activation energy (137kJ/mol or 101 kJ/mol). The *Stage 2* mass gain following drying at 130° is interpreted as due to chemisorbed water removed during heating. This is supported by a related water removal event in the TG-MS data, distinct from a lower temperature physisorption event and a higher temperature event associated with dehydroxylation.

- *The Stage 2 mass gain rates (rate constants) of the 130°C and 500°C curves are linearly related, with a fundamental connection between the underlying chemisorption events suggested:*

  A strong linear relationship, independent of the aging temperature, was found between the *Stage 2* mass gain rates (rate constants) following drying (130°C) and reheating (500°C) with ratio between the rates of approximately 1.25-1.30. A possible explanation is that the chemisorption event associated with 130°C has a fundamental relationship to that associated with 500°C reheating (rehydroxylation), with both events having an almost constant ratio of chemisorption sites across different samples due to some shared (mineralogical) component.

- *Further support for a $t^{1/n}$ model*:

  Strong support was found for the use of a $t^{1/n}$ model to describe the *Stage 2* mass gain behavior of samples, with $1/n$ = 1/6-1/2, dependent on the sample and in support of other work.[7-10] The $1/n$ variable has similar values following drying and reheating, regardless of aging temperature and a relationship was observed between the level of $1/n$ and the surface area/pore volume of the sample suggesting a connecting between the diffusion mechanism and the pore structure.

Many of the key assumptions and properties of RHX dating have come under criticism and more intense scrutiny to the point where the potential of the method is no longer clear. The above work clarifies and helps provide a better understanding and description of the underlying mass gain behavior and processes, necessary in order to assess whether an alternative or improved methodology is possible and how this might be applied in future work.

Acknowledgments

This work was conducted as part of Ph.D. research made possible through the aid of a Department for Employment and Learning (DEL) Ph.D. studentship for which I am grateful; a URL to the accessible digital version is provided in the references below. Acknowledgements are also made of the assistance provided by the School of Geography, Archaeology and Palaeoecology where this research was conducted. I wish to thank the following persons both for aiding source and for providing samples: Prof. Caroline Malone (QUB), Mr. Michael Barrett (Turlough), Dr. Joanne Curran (Consarc Design Group), Mr. Peter Francis (Ballynahinch), Ms. Audrey Gahan (Gahan and Long Arch. Serv. Ltd), Mr. Stephen Gilmore (Northern Arch. Cons. Ltd), Mr. Barrie Hartwell (GAP, QUB), Mr. Paul Logue (N. Ireland Environment Agency), Dr. Sara Pavía (Trinity College Dublin), Mr. Cormac McSparron and Mr. Ruairí Ó Baoill (Centre for Archaeological Fieldwork, QUB). For technical assistance and advice, I thank the following persons: Mr. Pat McBride (QUB), Mr. John Meneely (QUB), Mr. Peter Gray, Mr. Stephen Roper, and Mr. Jim McDonald (^{14}CHRONO Centre, QUB), Dr. Jennifer McKinley (GAP, QUB), Dr. John Caulfield (SPACE, QUB), Dr. Rory Flood (GAP, QUB), Mr. Mark Russell (SPACE, QUB) Mr. William Harra (ASEP, QUB).

I also wish to thank Prof. Paula Reimer for her helpful comments with regard to preparation of this text.

References

[1] M. A. Wilson, M. A. Carter, W. D. Hoff, C. Ince, S. D. Savage, B. McKay, and I. M. Betts, "Dating Fired-Clay Ceramics Using Long-Term Power Law Rehydroxylation Kinetics," *Proc. R. Soc. London, A*, **465**, 2407–15 (2009).

[2] M. A. Wilson, A. Hamilton, C. Ince, M. A. Carter, and C. Hall, "Rehydroxylation (RHX) Dating of Archaeological Pottery," *Proc. R. Soc. A.*, **468**, 3476–93 (2012).

[3] S. D. Savage, M. A. Wilson, M. A. Carter, W. D. Hoff, C. Hall, and B. McKay, "Moisture Expansion and Mass Gain in Fired Clay Ceramics: A Two-Stage (Time)$^{1/4}$ Process," *J. Phys. D: Appl. Phys.*, **41**, 055402 (2008).

[4] S. D. Savage, M. A. Wilson, M. A. Carter, B. McKay, W. D. Hall and C. Hall, "Mass Gain Due to the Chemical Recombination of Water in Fired Clay Brick," *J. Am. Ceram. Soc.*, **91**, 3396-3398 (2008).

[5] P. K. Bowen, H. J. Ranck, T. J. Scarlett, and J. W. Drelich, "Rehydration/Rehydroxylation Kinetics of a Reheated XIX-Century Davenport (Utah) Ceramic," *J. Am. Ceram. Soc.*, **94**, 2585–91 (2011).

[6] P.K. Bowen, J. Drelich, and T. J. Scarlett, "Modeling Rehydration/Rehydroxylation Mass-gain Curves from Davenport Ceramics. *J. Am. Ceram. Soc.*, **96**, 885-891 (2013).

[7] M. Le Goff and Y. Gallet, "Evaluation of the Rehydroxylation Dating Method: Insights from a New Measurement Device," *Quat. Geochronol*. **20**, 89–98, doi: 10.1016/j.quageo.2013.12.001 (2014).

[8] M. Le Goff and Y. Gallet, "Evidence for Complexity in the RHX Dating Method," *Archaeometry*, **57** (5) 897-910, doi: 10.1111/arcm.12137 (2015).

[9] M. Le Goff and Y. Gallet, "Experimental Variability in Kinetics of Moisture Expansion and Mass Gain in Ceramics," *J. Am. Ceram. Soc.*, **98**, 398–401 (2015).

[10] Y. Gallet and M. Le Goff, "Rehydration and Rehydroxylation in Ancient Ceramics: New Constraints from Mass Gain Analyses versus Annealing Temperatures," *J. Am. Ceram. Soc.*, **98**, 2738-2744 (2015).

[11] G. T. Barrett, "Rehydroxylation Dating: Assessment for Archaeological Application"; Ph. D. Thesis, Queen's University Belfast, April 2015. Digital version online: http://pure.qub.ac.uk/portal/en/publications/rehydroxylation-dating-assessment-for-archaeological-application(9c89d2bd-ceaf-4f3d-a9d0-515eb23e6204).html

[12] C. M. Stevenson, and M. Gurnick, "Structural Collapse in Kaolinite, Montmorillonite and Illite Clay and its role in the Ceramic Rehydroxylation Dating of Low-fired Earthenware," *J. Archaeol. Sci.*, **69,** 54-63 (2016).

[13] A. Hamilton, and C. Hall, "A Review of Rehydroxylation in Fired-clay Ceramics," *J. Am. Ceram. Soc.*, **95,** 2673-2678 (2012).

[14] F. S. Baker, and K. S. W. Sing, "Specificity in the adsorption of nitrogen and water on hydroxylated and dehydroxylated silicas," *J. Colloid Interface Sci.* **55**, 605-613 (1976).

[15] P. M. Rice, "Pottery Analysis: a Sourcebook," University of Chicago Press, Chicago, (1987).

[16] P. S. Quinn, "Ceramic Petrography: The Interpretation of Archaeological Pottery & Related Artefacts in Thin Section," Archaeopress, Oxford, (2013). [Chapter 3]

[17] M. A. Wilson, S. Clelland, M. A. Carter, C. Ince, C. Hall, A. Hamilton. and C. M. Batt, "Rehydroxylation of Fired-Clay Ceramics: Factors Affecting Early-Stage Mass Gain in Dating Experiments," *Archaeometry*, **56**, 689–702 (2014).

[18] F. Clegg, C. Breen, M. A. Carter, C. Ince, S. D. Savage, and M. A. Wilson, "Dehydroxylation and Rehydroxylation Mechanisms in Fired Clay Ceramics: A TG-MS and DRIFTS Investigation," *J. Am. Ceram. Soc*., **95**, 416–22 (2012)

[19] A. C. Dunham, "Developments in Industrial Mineralogy: I. The Mineralogy of Brick-making." *Proceedings of the Yorkshire Geological Society.* **49** 95-104 (1992)

[20] G. T. Barrett, "Rehydroxylation Dating of Fired Clays: an Improved *time-offset* Model to account for the Effect of Cooling on Post-Reheating Mass Gain," *J. Archaeol. Sci.,* **40**, 3596-3603 (2013)

[21] L. Greenspan, "Humidity Fixed Points of Binary Saturated Aqueous Solutions," *J. Res. Natl. Bur. Stand. Sec. A.,* **81A**, 89-96 (1976)

[22] C. Hall and W. D. Hoff, "Moisture Expansivity of Fired-clay Ceramics," *J. Am. Ceram. Soc.,* **95**, 1204-1207 (2012).

[23] C. Hall, A. Hamilton, and M. A. Wilson, "The Influence of Temperature on Rehydroxylation [RHX] Kinetics in Archaeological Pottery," *J. Archaeol. Sci.,* **40**, 305-312 (2013)

[24] S. Lowell, J. E. Shields, and M. A. Thomas, "Characterization of Porous Solids and Powders: Surface Area, Pore Size and Density," Kluwer Academic Publishers, Dordrecht, (2004) [Chapter 4]

[25] H. Mesbah, M. A. Wilson and M. A. Carter, "Effect of Prolonged Sintering Time at 1200°C on the Phase Transformation and Reactivity with Moisture of Fired Kaolinite" *11th International Conference on Ceramic Processing Science*. 27th August (2010).

[26] S. Zhao, P. K. Bowen, J. W. Drelich and T. J. Scarlett, "Reproducibility in Rehydroxylation of Ceramic Artifacts," *J. Am. Ceram. Soc.,* **98**, 3367-3372 (2015).

[27] S. J. Clelland, M. A. Wilson, M. A. Carter, and C. M. Batt, "RHX Dating: Measurement of the Activation Energy of Rehydroxylation for Fired-Clay Ceramics," *Archaeometry*, **57,** 392-404, doi: 10.1111/arcm.12118 (2015).

[28] V. A. Drits and D. K. McCarty, "The Nature of Structure-Bonded H_2O in Illite and Leucophyllite from Dehydration and Dehydroxylation Experiments," *Clays Clay Miner*., **55** [1] 45–58 (2007)

Figure Captions:

Figure 1: (a) Mass gain behaviour, *Stage 1* and *Stage 2* related notation, following reheating of a ceramic. Dash-dot curved lines illustrate *positive* or *negative* curvature. (b) *Stage 2* mass gain rate components (and intercept masses) following drying to constant mass at 130°C (blue) and following reheating at 500°C (red). The mass gain rate following heating at 500° is the sum of two components, the mass gain due to processes related to drying at 130°C (chemisorption processes) plus the processes related to heating between 130-500°C (RHX attributed here for simplicity but see discussion).

Figure 2: Mass gain curves, displaying the *Stage 1* (and *Stage 2*) region, of *Ann, Esp, Rom, Mac, Rat, Lan* (clockwise from top left) samples. Sample aging at 25°C following heating at 130°C (blue circles) and 500°C (red squares).

Figure 3: Fractional mass gain curves (*Stage 2*) of *Ann, Ria, Joy, Lan* (*a-d*) samples, following heating at 130°C (blue) and 500°C (red) and aging at temperatures of 25°C (square), 35°C (triangle), and 45°C (circle). Dashed lines correspond to linear fits with the exception of *Lan* (interpolation) where fitting was not possible.

Figure 4: (a) Comparison of *S1* fractional mass for 130°C and 500°C components with abnormal samples and additionally *Mac, Cau,* and *Bel* removed. For the $t^{1/4}$ model. (b) Mass gain rate of drying at 130°C (25°C, 35°C, 45°C aging) versus reheating at 500°C (25, 35, 45°C aging) with abnormal samples excluded. Using $t^{1/4}$ model. (c) Arrhenius plot ($t^{1/4}$ model) for 130°C (blue), 500°C (red) and RHX (green) components of mass gain rates for *Ann.* Uncertainties are to 2σ.

Figure 5: (a) Activation energies calculated for 130°C (blue) and 500°C (red) components, for $t^{1/4}$ model (left). Included are the uncertainties (2σ). (b) RHX activation energy and uncertainties (2σ) for $t^{1/4}$ model.

Figure 6: (a) Curvature (*1/n*) of samples for drying (130°C, average of 3 aging temperatures), reheating (500°C, average of 3 aging temperature), and the combined averages of both. Uncertainties to 1 standard deviation. (b) BET surface areas of samples. Value of 0.0 for *Rat* corresponds to negligible adsorption. (c) *S1* fractional mass gain versus BET S.A. for all samples ($t^{1/4}$) model. (d) Relationship between BET S.A. and 1/*n* of samples.

Figure 7: TG-MS for mass 18 ion (H_2O^+) removal during heating. Black curve – average H_2O removal curve for 10 well-behaved samples (excluding *Mac* and *Bel*). Red dashed – the 1σ variability of this average. Red dotted – individual curve for *Rat.* Green dashed – individual curve for *Ann*.

Tables:

Table 1: TG-MS analysis summary. Peaks (corresponding to events *A*-*D*) attributed to H_2O loss are color coded (also type bold/normal weak) according to strength of visible structure (numbers are in °C).

	H_2O peaks (yellow/italic = weak, orange/normal = medium, red/bold =strong)			
Event	***A***	***B***	***C***	***D***
Ann	**70**	130	-	**310**
Esp	**60-70**	*110*	260-270	-
Nic	50	-	**210-230**	-
Mac	**90**	-	-	310-320
Ria	50	*120-160*	-	**320-330**
Etr	**90**	-	240	-
Rom	**90-100**	-	230-240	-
Por	**60-70**	-	-	*310-340*
Rat	*60*	**160-170**	-	**350**
Cal	**60**	140	-	**340-350**
Lan	**90**	-	*210*	*350-400*
Joy	*60*	150	-	**310-320**
Cau	70	**130-140**	*270-280*	-
Bel	**90-100**	-	*250-300*	-
Dow1	**80-90**	-	*200-250*	340-390
Dow2	**95-110**	-	-	**350-400**
Tur	60-70	140-160	-	**310-330**
Ted	-	170-180	-	**290-310**

Figures:

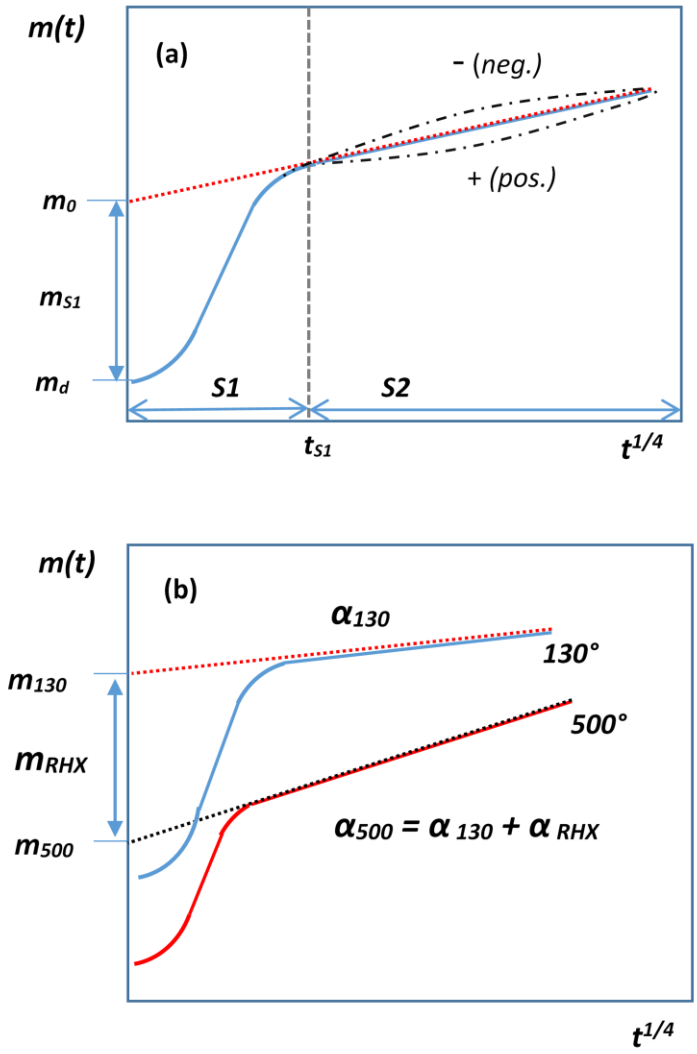

Figure 1: (a) Mass gain behaviour, *Stage 1* and *Stage 2* related notation, following reheating of a ceramic. Dash-dot curved lines illustrate *positive* or *negative* curvature. (b) *Stage 2* mass gain rate components (and intercept masses) following drying to constant mass at 130°C (blue) and following reheating at 500°C (red). The mass gain rate following heating at 500° is the sum of two components, the mass gain due to processes related to drying at 130°C (chemisorption processes) plus the processes related to heating between 130-500°C (RHX attributed here for simplicity but see discussion).

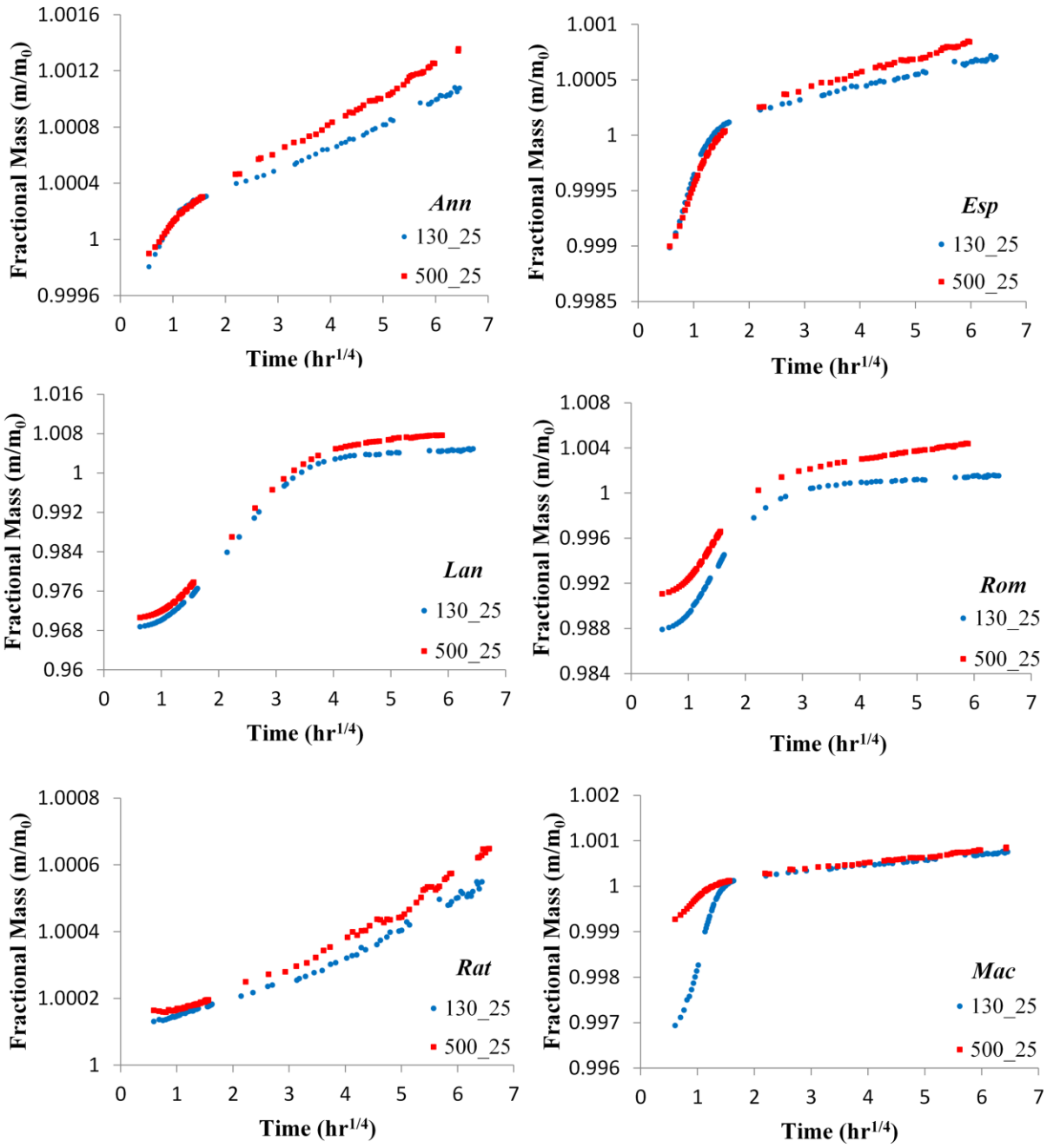

Figure 2: Mass gain curves, displaying the *Stage 1* (and *Stage 2*) region, of *Ann*, *Esp*, *Rom*, *Mac*, *Rat*, *Lan* (clockwise from top left) samples. Sample aging at 25°C following heating at 130°C (blue circles) and 500°C (red squares).

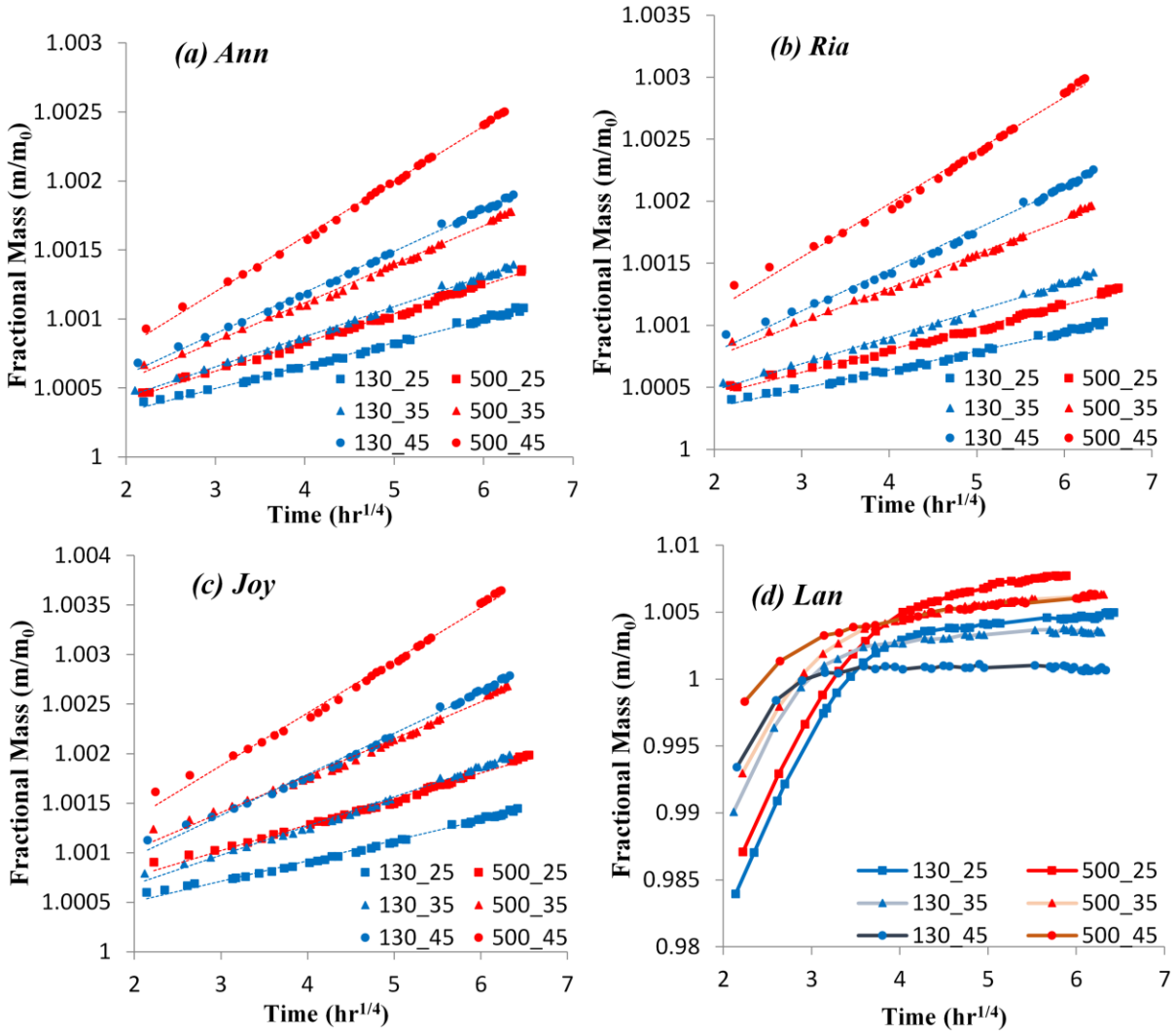

Figure 3: Fractional mass gain curves (*Stage 2*) of *Ann, Ria, Joy, Lan* (*a-d*) samples, following heating at 130°C (blue) and 500°C (red) and aging at temperatures of 25°C (square), 35°C (triangle), and 45°C (circle). Dashed lines correspond to linear fits with the exception of *Lan* (interpolation) where fitting was not possible.

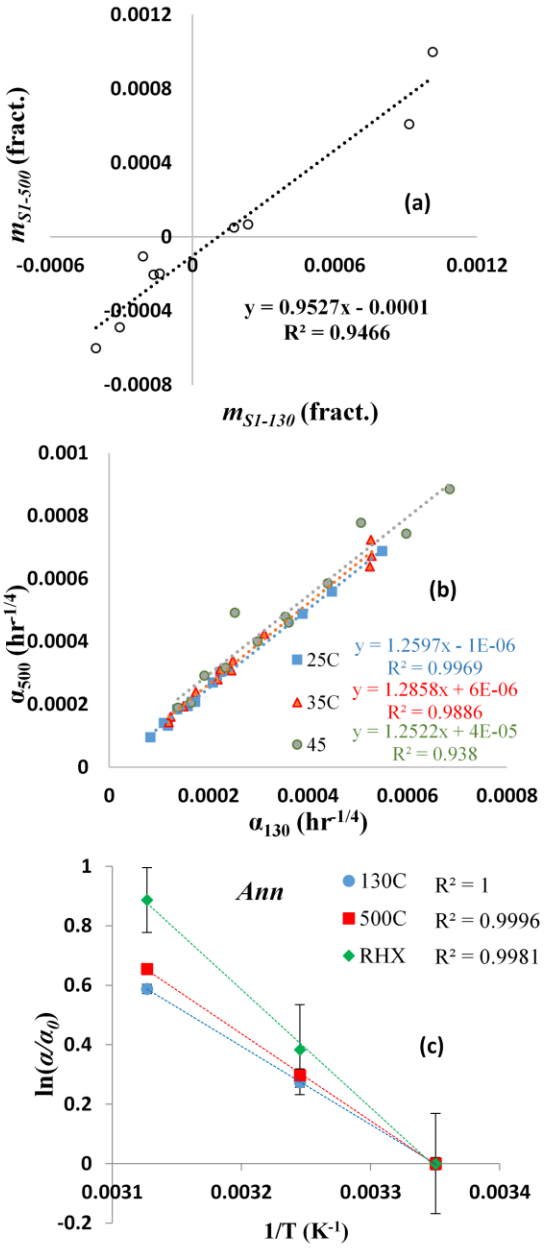

Figure 4: (a) Comparison of *S1* fractional mass for 130°C and 500°C components with abnormal samples and additionally *Mac*, *Cau*, and *Bel* removed. For the $t^{1/4}$ model. (b) Mass gain rate of drying at 130°C (25°C, 35°C, 45°C aging) versus reheating at 500°C (25, 35, 45°C aging) with abnormal samples excluded. Using $t^{1/4}$ model. (c) Arrhenius plot ($t^{1/4}$ model) for 130°C (blue), 500°C (red) and RHX (green) components of mass gain rates for *Ann*. Uncertainties are to 2σ.

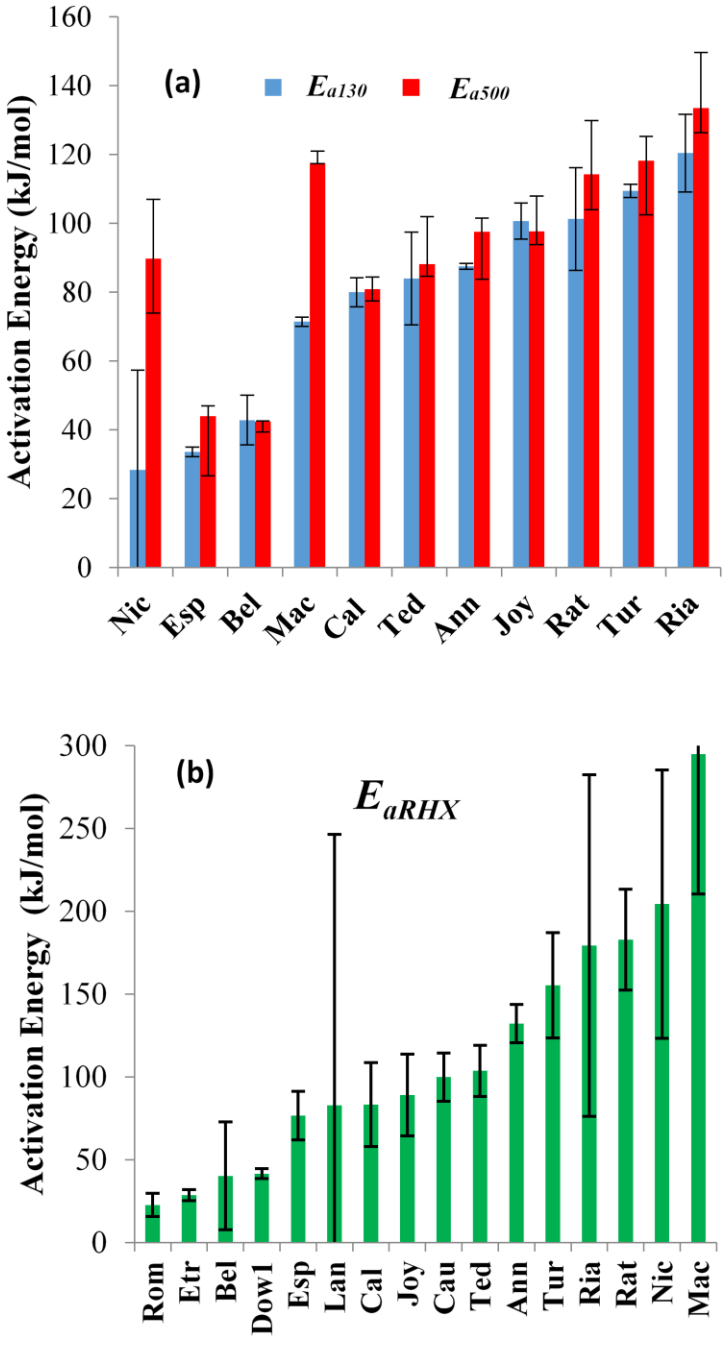

Figure 5: (a) Activation energies calculated for 130°C (blue) and 500°C (red) components, for $t^{1/4}$ model (left). Included are the uncertainties (2σ). (b) RHX activation energy and uncertainties (2σ) for $t^{1/4}$ model.

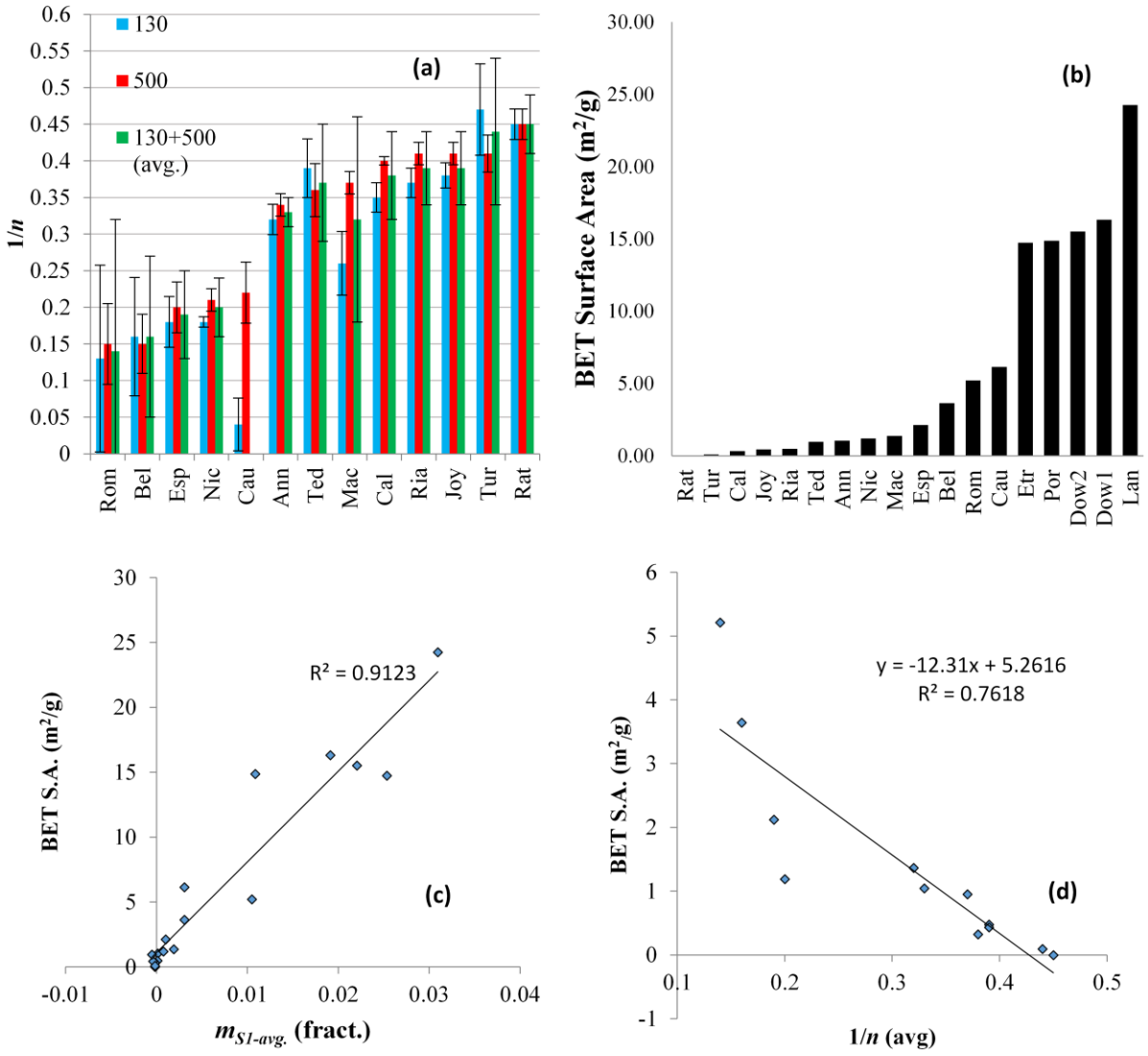

Figure 6: (a) Curvature (*1/n*) of samples for drying (130°C, average of 3 aging temperatures), reheating (500°C, average of 3 aging temperature), and the combined averages of both. Uncertainties to 1 standard deviation. (b) BET surface areas of samples. Value of 0.0 for *Rat* corresponds to negligible adsorption. (c) *S1* fractional mass gain versus BET S.A. for all samples ($t^{1/4}$) model. (d) Relationship between BET S.A. and 1/*n* of samples.

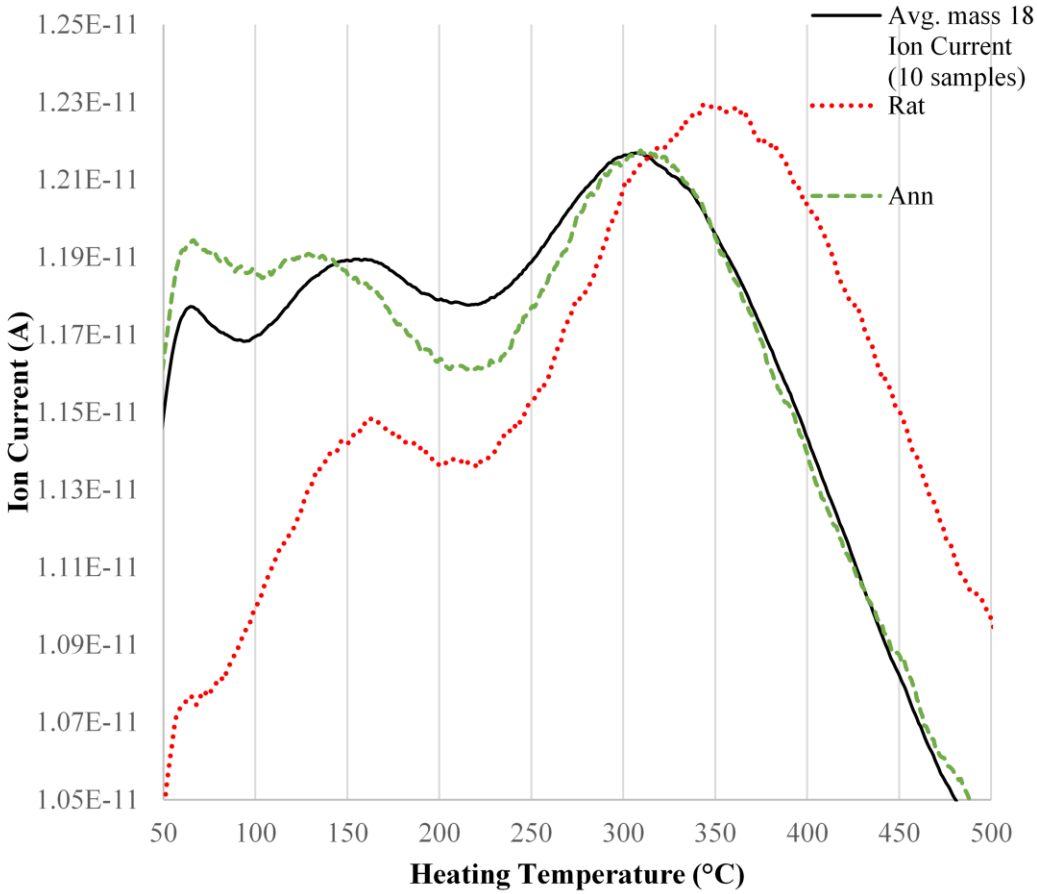

Figure 7: TG-MS for mass 18 ion (H_2O^+) removal during heating. Black curve – average H_2O removal curve for 10 well-behaved samples (excluding *Mac* and *Bel*). Red dashed – the 1σ variability of this average. Red dotted – individual curve for *Rat*. Green dashed – individual curve for *Ann*.